

# Comparative Study on Si and Ge p-type Nanowire FETs based on Full-Band Non-Equilibrium Green's Function Simulation

Hideki Minari and Nobuya Mori

Division of Electrical, Electronic and Information Engineering  
 Graduate School of Engineering, Osaka University  
 2-1 Yamada-oka, Suita City, Osaka 565-0871, Japan  
 Email: minari@si.eei.eng.osaka-u.ac.jp

**Abstract**—Atomistic hole transport simulation based on a nonequilibrium Green's function method and tight-binding approximation has been performed for Si and Ge p-type nanowire FETs with the diameter ranging from 1.6 nm to 3 nm. Simulation results show that the drain current density increases with increasing the nanowire diameter and the difference in drain current between Ge and Si nanowire FETs becomes smaller with reducing the nanowire diameter.

**Keywords**—Silicon; Germanium; Nanowire; NEGF method; Tight-binding; Simulation

## I. INTRODUCTION

Nanowire (NW) field-effect-transistors (FETs) are considered to be one of the most promising device structures that provide effective gate-control even at the nanoscale. It is well-known that germanium (Ge) has lighter hole effective mass and higher hole mobility compared to those of silicon (Si). Ge p-type MOSFETs are considered to be an attractive candidate for high performance devices. For p-type NW FETs, however, confinement-induced mixing of heavy-hole and light-hole states [1] makes the subband dispersion quite nonparabolic [2]. It is, therefore, not clear from the bulk energy-band structure which channel materials exhibit superior device characteristics for p-type NW FETs. To address this issue, quantum-mechanical computations including full-band structures are required. Nonequilibrium Green's function (NEGF) method [3]–[6] allows one to perform quantum transport simulation in ultra-small MOSFETs. By combining the NEGF method with an empirical tight-binding approximation (TBA), quantum-mechanical computations including full-band structures can be achieved [5], [7]. In the present study, we have simulated device characteristics of Si and Ge p-type NW FETs within a framework of three-dimensional NEGF formalism and an empirical TBA to obtain quantitative understanding energy-band structure effects on drain current of p-type NW FETs.

## II. SIMULATION METHOD

We consider p-type gate-all-around NW FETs with a gate-length of 3.4 nm and insulator-thickness of 1 nm, whose schematic diagram is given in Fig. 1. The channel materials are

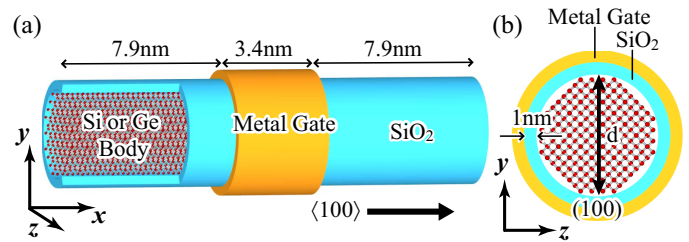


Fig. 1. (a) Schematic diagram of a gate-all-around NW FET structure and (b) the cross sectional view.

Si or Ge with the diameter  $d$  ranging from 1.6 nm to 3 nm. The NW axis ( $x$ -direction) is along a  $\langle 100 \rangle$  crystalline orientation. The doping concentration in the source and drain regions, each of which is  $7.9 \text{ nm}$  long, is  $5 \times 10^{19} \text{ cm}^{-3}$ . To compare the device performance originated in channel materials, we assume that the gate consists of a fictitious metal whose Fermi energy coincides with the lowest subband level of the NW and the insulator consists of  $\text{SiO}_2$  for both Si and Ge NWs.

We take into account the full-band structure within an empirical  $sp^3s^*$  nearest-neighbor TBA [8], [9] including five

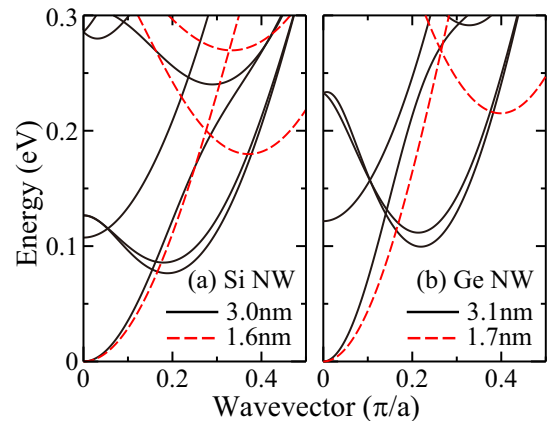


Fig. 2. Subband energies of (a) Si NWs and (b) Ge NWs with a diameter of  $d = 3 \text{ nm}$  (solid line) and  $d = 1.6 \text{ nm}$  (dashed line).

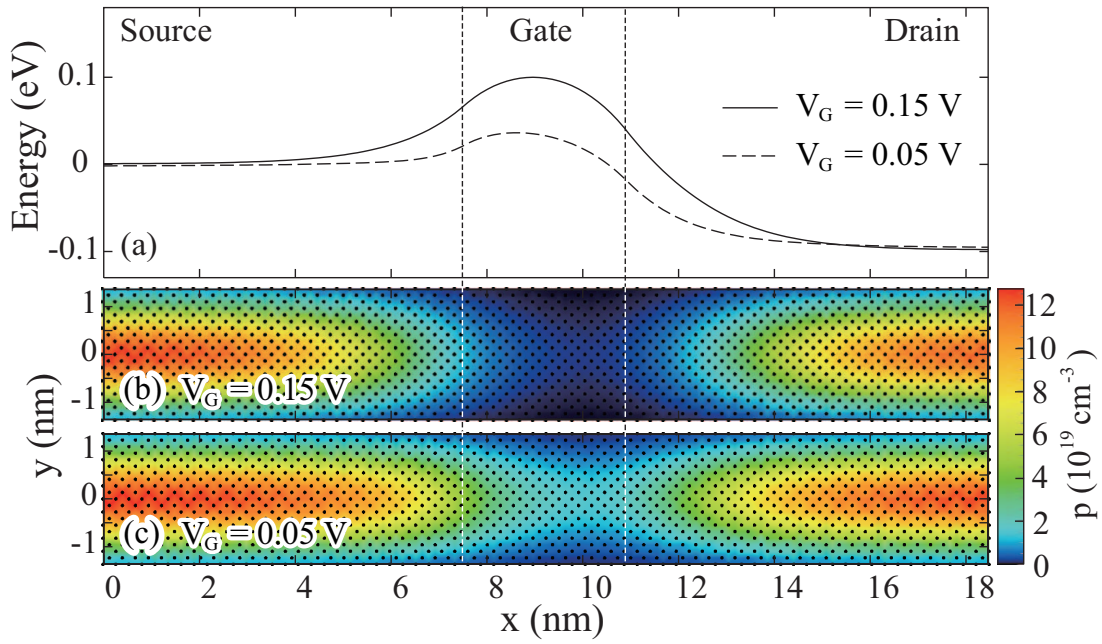


Fig. 3. (a) Potential profiles of Si NW FET with  $d = 3.0$  nm at  $V_D = 0.1$  V and  $T = 300$  K for  $V_G = 0.15$  V (solid line) and  $V_G = 0.05$  V (dashed line). Corresponding two-dimensional hole density profiles for (b)  $V_G = 0.15$  V and (c)  $V_G = 0.05$  V. Black dots represent the Si atomic positions.

orbitals without the spin-orbit coupling. We treated the semiconductor/insulator interfaces with the H termination model [10], [11] to eliminate the artificial surface states in the energy region of interest. Figure 2 shows the subband dispersion of Si and Ge NWs with a diameter of  $d = 3$  nm and  $d = 1.6$  nm. The nonparabolicity of the subband is tremendous due to the strong confinement-induced mixing of heavy-hole and light-hole states. The energy minimum of the lowest subband locates at  $k = 0$ , while those of some higher subbands locate at off  $k = 0$  (we call those subbands “off-valley subband” hereinafter). The effective mass of the lowest subband of Ge NW is significantly smaller than that of Si NW.

We calculate hole current using the NEGF method [3]–[6]. In the present study, we neglect scattering and assume ballistic transport. The potential profiles are obtained through a self-consistent solution of three-dimensional Poisson and NEGF equations.

### III. RESULTS AND DISCUSSION

Figure 3(a) shows the potential profiles of Si NW FET with  $d = 3.0$  nm at  $V_D = 0.1$  V and  $T = 300$  K for  $V_G = 0.15$  V and  $0.05$  V. Figures 3(b) and 3(c) show the corresponding two-dimensional hole density profiles for  $V_G = 0.15$  V and  $V_G = 0.05$  V, respectively. Black dots represents the Si atomic positions. We considered 5,891 atoms in the calculation domain. Figure 4 shows transfer characteristics of Si and Ge NW FETs with  $d = 1.6$  nm. The subthreshold swings of Si and Ge NW FETs are 62.4 mV/dec and 61.6 mV/dec, respectively, showing that both devices maintain a good gate control with an almost ideal subthreshold swing.

Figures 5 and 6 show the hole density spectra, current spectra, and potential profiles of Si and Ge NWs, respectively,

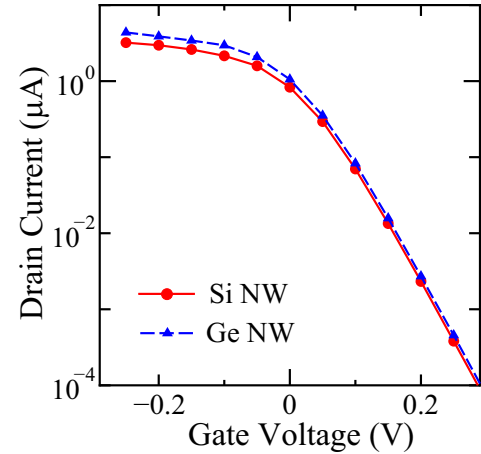


Fig. 4. Drain-current–gate-voltage characteristics of Si NW FET (solid line) and Ge NW FET (dashed line) with  $d = 1.6$  nm at  $V_D = 0.1$  V.

with  $d = 3.0$  nm at  $V_D = 0.1$  V,  $V_G = 0.1$  V, and  $T = 300$  K. Since Ge NW has lighter effective mass, the hole density distribution is wider in energy space (see Fig. 2).

Figure 7 shows the NW diameter dependence of (a) drain current  $I_D$  (b) and drain current density  $J_D$  from  $d = 1.6$  nm to 3 nm. The drain current density  $J_D$  increases with increasing the NW diameter. This is because thicker NWs have lighter effective masses (see Fig 2). However, for Si NW FET with  $d = 1.6$  nm, the drain current density is larger than that with  $d = 1.9$  nm. Figures 8 and 9 show the hole density spectra and subband structures of the devices with  $d = 1.6$  nm and  $d = 1.9$  nm, respectively. Since the off-valley subband level locates higher energies for  $d = 1.6$  nm, the drain current

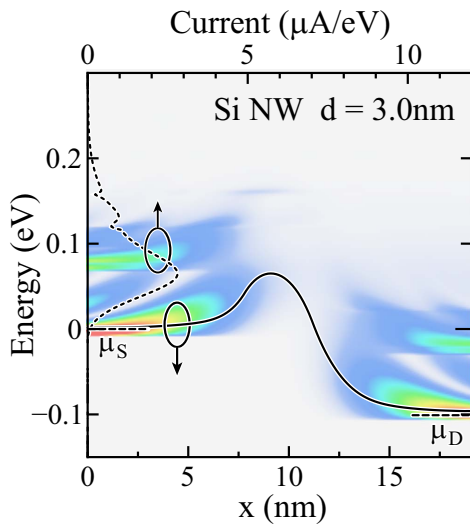


Fig. 5. Local hole density spectrum (density plot) of Si NW FET with  $d = 3 \text{ nm}$  at  $V_D = 0.1 \text{ V}$  and  $V_G = 0.1 \text{ V}$ . Solid line shows potential profile, dotted line current spectrum, and dashed lines the Fermi levels in the source ( $\mu_S$ ) and drain ( $\mu_D$ ) regions.

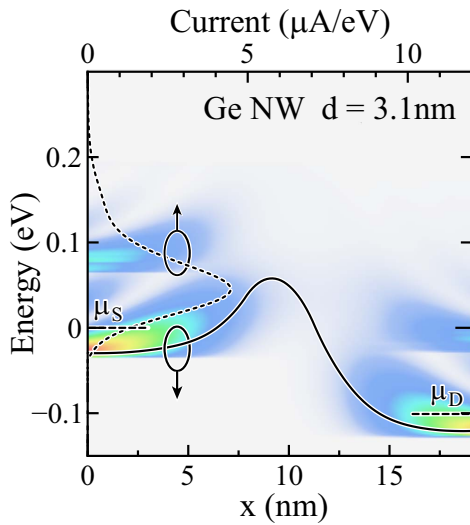


Fig. 6. The same as Fig. 5 but for Ge NW FET.

density of Si NW with  $d = 1.6 \text{ nm}$  is determined mainly by the lowest subband. On the other hand, for  $d = 1.9 \text{ nm}$ , the off-valley subband level becomes lower and contributes to the drain current. The effective mass of the off-valley subband is quite large resulting in the drain current density reduction in Si NW with  $d = 1.9 \text{ nm}$  compared to that in Si NW with  $d = 1.6 \text{ nm}$ .

Figure 10 shows the drain current ratio between Si and Ge NW FETs as a function of the NW diameter from  $d = 1.6 \text{ nm}$  to  $3 \text{ nm}$ . For  $d = 3.0 \text{ nm}$ , the drain current of Ge NW FET is 58 percent larger than that of Si NW FET. This can be attributed to the smaller effective mass of Ge NW. However, for  $d = 1.6 \text{ nm}$ , the drain current of Ge NW FET is only 19 percent larger than that of the Si NW FET. This is because the

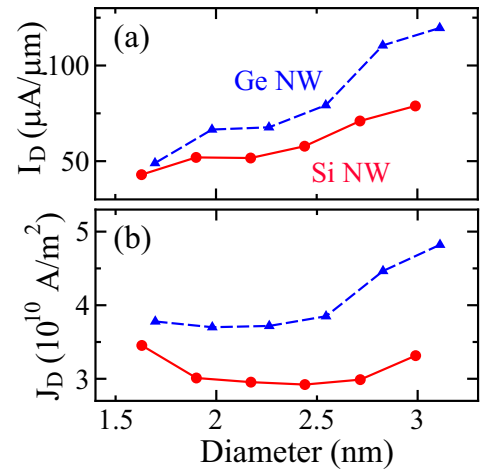


Fig. 7. (a) Drain current  $I_D$  and (b) drain current density  $J_D$  versus NW diameter  $d$  for Si NW FETs (solid line) and Ge NW FETs (dashed line) at  $V_D = 0.1 \text{ V}$  and  $V_G = 0.1 \text{ V}$ .  $I_D$  is normalized by an effective gate width  $d$ .

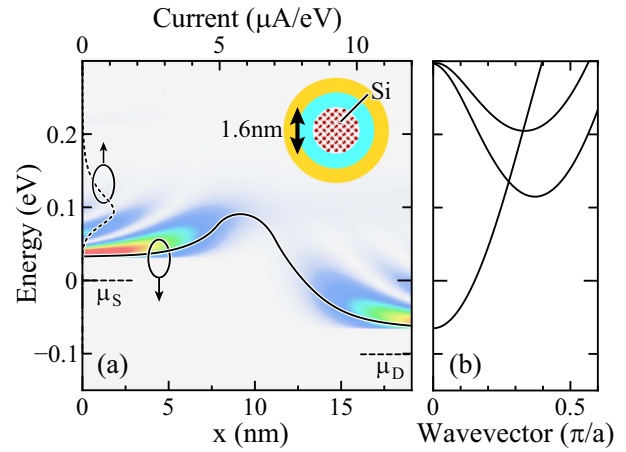


Fig. 8. (a) The same as Fig. 5 but for  $d = 1.6 \text{ nm}$ . (b) Subband structure at the drain contact.

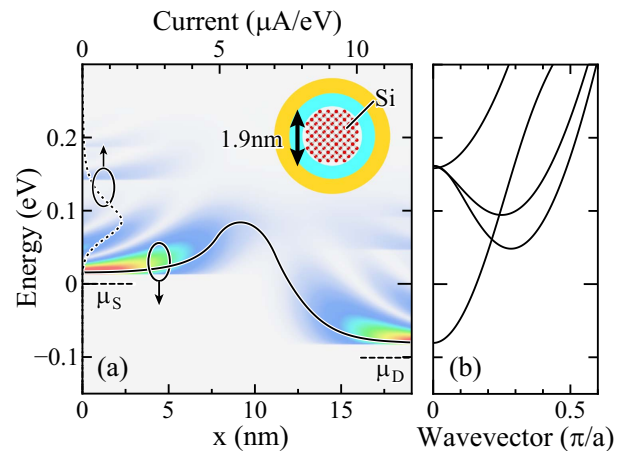


Fig. 9. The same as Fig. 8 but for  $d = 1.9 \text{ nm}$ .

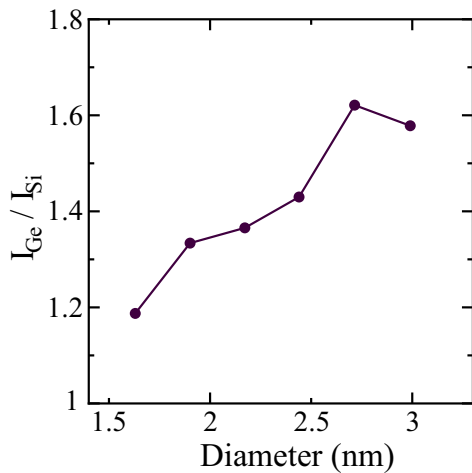


Fig. 10. Drain-current ratio between Ge and Si NW FETs as a function of the NW diameter  $d$ .  $V_D = 0.1$  V and  $V_G = 0.1$  V.

difference in effective masses of the lowest subband between Ge and Si NWs becomes smaller with reducing the NW diameter.

#### IV. CONCLUSION

Hole transport simulation based on the NEGF and TBA methods has been performed for Si and Ge NW FETs. We found that the drain current density increases with increasing the NW diameter and the difference in drain current between Ge and Si NWs becomes smaller with reducing the NW diameter.

#### ACKNOWLEDGMENT

This work was supported by the Semiconductor Technology Academic Research Center (STARC) and the Global COE Program "Center for Electronic Devices Innovation" (CEDI).

#### REFERENCES

- [1] C. Weisbuch, *Fundamental Properties of III-V Semiconductor Two-Dimensional Quantized Structures: The Basis for Optical and Electronic Device Applications*, R. Dingle, ed., *Semicond. Semimet.* **24**, 1 (1987).
- [2] H. Minari and N. Mori, "Crystalline orientation effects on ballistic hole current in ultrathin DG SOI MOSFETs," *Simulation of Semiconductor Processes and Devices 2007*, edited by T. Grassler and S. Selberherr, pp. 229-232 (2007).
- [3] S. Datta, *Electronic Transport in Mesoscopic Systems*, (Cambridge University Press, Cambridge, UK, 1995).
- [4] H. Haug and A.-P. Jauho, *Quantum Kinetics in Transport and Optics of Semiconductors* (Springer, Berlin, 1996).
- [5] A. Pecchia and A. Di Carlo, "Atomistic theory of transport in organic and inorganic nanostructures," *Rep. Prog. Phys.*, **67**, 1497 (2004).
- [6] M. Lundstrom and J. Guo, *Nanoscale Transistors: Device Physics, Modeling, and Simulation* (Springer, New York, 2006).
- [7] M. Luisier, A. Schenk, W. Fichtner, and G. Klimeck, "Atomistic simulation of nanowires in the  $sp^3d^5s^*$  tight-binding formalism: From boundary conditions to strain calculations," *Phys. Rev. B*, **74**, 205323 (2006).
- [8] P. Vogl, H.P. Hjalmarson, and J.D. Dow, "A semi-empirical tight-binding theory of the electronic structure of semiconductors," *J. Phys. Chem. Solids*, **44**, 365 (1983).
- [9] A.V. Podolskiy and P. Vogl, "Compact expression for the angular dependence of tight-binding Hamiltonian matrix elements," *Phys. Rev. B*, **69**, 233101 (2004).
- [10] S. Lee, F. Oyafuso, P. von Allmen, and G. Klimeck, "Boundary conditions for the electronic structure of finite-extent embedded semiconductor nanostructures," *Phys. Rev. B*, **69**, 045316 (2004).
- [11] Y. Zheng, C. Rivas, R. Lake, K. Alam, T.B. Boykin, and G. Klimeck, "Electronic properties of silicon nanowires," *IEEE Trans. Nanotech.*, **52**, 1097 (2005).